Available online at www.sciencedirect.com
SCIENCE DIRECT
Journal of Non-Crystalline Solids 352 (2006) 2371–2375
JOURNAL OF NON-CRYSTALLINE SOLIDS
www.elsevier.com/locate/jnoncrysol

Continuous-wave laser operation of disordered double tungstate and molybdate crystals doped with ytterbium

V. Petrov [a,*], M. Rico [a], J. Liu [a], U. Griebner [a], X. Mateos [a], J.M. Cano-Torres [b], V. Volkov [b], F. Esteban-Betegón [b], M.D. Serrano [b], X. Han [b], C. Zaldo [b]

[a] *Max-Born-Institute for Nonlinear Optics and Ultrafast Spectroscopy, A3 Department, 2A Max-Born-Str., D-12489 Berlin, Germany*
[b] *Instituto de Ciencia de Materiales de Madrid (ICMM), CSIC, c/ Sor Juana Inés de la Cruz 3, Cantoblanco, E-28049 Madrid, Spain*

Available online 16 May 2006

Abstract

Several ytterbium doped disordered doubles tungstate and molybdate crystals, $NaGd(WO_4)_2$, $NaLa(WO_4)_2$, $NaLa(MoO_4)_2$ and $LiGd(MoO_4)_2$, were grown with sufficient Yb-doping and optical quality. The crystal field splitting of the Yb^{3+} multiplets and the lifetimes are similar to the biaxial monoclinic double tungstates but the peak absorption cross sections are roughly one order of magnitude lower. Room temperature cw laser operation was achieved under Ti:sapphire and diode laser pumping. The polarization dependence of the laser emission and possible power scaling were studied. The slope efficiency achieved with the best sample, $Yb:LiGd(MoO_4)_2$, was 64.5%. The maximum output power obtained was 900 mW for $Yb:NaLa(MoO_4)_2$ pumped in the absorption maximum. The laser tunability was studied with an intracavity Lyot filter and the tuning ranges (FWHM up to 33 nm) achieved indicate interesting potential for mode-locked femtosecond operation.

PACS: 42.55.Rz; 42.55.Xi; 42.70.Hj

Keywords: Crystal growth; Lasers

1. Introduction

Double tungstate and molybdate compounds with the general formula $MT(XO_4)_2$ where M is a monovalent alkali cation (Li–Cs), T is a trivalent cation (Al, Ga, In, Cr, Bi, Y, La or lanthanide Ln = Ce–Lu), and X = W or Mo, may exhibit ordered phases with separate sites for M and T cations and disordered phases where M and T cations are randomly distributed over the same cationic sublattice [1]. Some of the optically passive ordered phases like the strongly anisotropic (biaxial) monoclinic $KGd(WO_4)_2$ and $KY(WO_4)_2$ are established rare-earth ion laser hosts with very large absorption and emission cross sections of the active dopant [2]. The disordered phases are, however, interesting because the inhomogeneous broadening extends the potential for tunable laser operation and generation of ultrashort optical pulses and also because their uniaxial character leads to less anisotropy in the opto-mechanical properties which is important for the processing of active elements and their thermal management. The disordered phases exhibit tetragonal structure and often congruent melting character. The latter allowed us to grow several Na-based tungstates and molybdates by the Czochralski method [3–7]. Although different Ln-dopants and dopant combinations were studied, we focused most of our recent activities on the Yb^{3+} ion which currently attracts considerable attention for the 1 μm spectral range as an alternative to the widely spread Nd^{3+} ion. Due to its strong electron–phonon coupling to the lattice, this ion exhibits linewidths which are intrinsically broader than the Nd^{3+} ion. Moreover, Yb^{3+} possesses longer energy-storage lifetime and smaller quantum defect (less heat generation)

* Corresponding author. Tel.: +49 30 63921272; fax: +49 30 63921289.
E-mail address: petrov@mbi-berlin.de (V. Petrov).

0022-3093/$ - see front matter © 2006 Elsevier B.V. All rights reserved.
doi:10.1016/j.jnoncrysol.2006.02.060

than Nd^{3+}, and it can be pumped by the optically more robust InGaAs diode lasers operating in the 900–1000 nm spectral range. Finally, the relatively simple two-manifold structure of Yb^{3+} prohibits undesired excited state absorption, up-conversion and cross-relaxation processes.

The first reports on laser activity of Yb^{3+} in disordered double tungstate or molybdate crystals appeared in 2004 [4] and the few subsequent publications were focused on a limited number of such hosts [4,5,8–11]. In this paper, we summarize our previous achievements with Yb-doped $NaGd(WO_4)_2$ (NaGdW), $NaLa(WO_4)_2$ (NaLaW), $NaLa(MoO_4)_2$ (NaLaMo), and present some new results with Yb-doped $LiGd(MoO_4)_2$ (LiGdMo) comparing the different hosts. All laser results reported were obtained at room temperature, operating in the continuous-wave (cw) mode and using either a Ti:sapphire or a diode laser for pumping.

2. Crystal growth and crystalline structure

The new Yb-doped LiGdMo crystal was grown by the Top Seeded Solution Growth method using Li_2MoO_4 as solvent. In this host the complete substitution of Gd by Yb has been previously demonstrated with the stoichiometric material $LiYb(MoO_4)_2$ [8]. The Yb-doped $NaT(XO_4)_2$ (T = Gd, La and X = W, Mo) single crystals were grown in air by the Czochralski method using 75 cm^3 Pt crucibles. Details on the crystal growth procedures can be found in [4–7]. Both in the Li-based and Na-based tungstates and molybdates the crystallization temperature decreased with increasing Yb concentration. Typical segregations coefficients $K = [Yb]_{crystal}/[Yb]_{melt}$, where [Yb] denotes the concentration, estimated by inductively coupled plasma (ICP) emission, were about 0.8 for NaGdW, 0.6 for NaLaW, 0.35–0.5 for NaLaMo, and 0.6 for LiGdMo. The Yb doping levels in these materials, reached in crystals with which lasing could be achieved, were 5.1×10^{20} cm^{-3} (NaGdW), 1.1×10^{20} cm^{-3} (NaLaW), 3.08×10^{20} cm^{-3} (NaLaMo), and 4.06×10^{20} cm^{-3} (LiGdMo). Typically the grown boules had sizes of several cm^3 from which good quality samples with a volume of 0.1–0.3 cm^3 could be cut and polished.

All these $MT(XO_4)_2$ compounds have a crystallographic structure related to that of tetragonal scheelite ($CaWO_4$) $I4_1/a$ (No. 88). Previously this same space group was ascribed in most of the cases to the crystals with local disorder. Our X-ray diffraction studies indicate, however, the presence of reflections not allowed by the $I4_1/a$ space group symmetry, e.g., [7]. These peaks, although of weak intensity, cannot be ignored as their intensity is clearly above the background noise. Their presence is accounted for by the assumption of the space group $I\bar{4}$ (No. 82). This latter crystal structure contains two kinds of XO_4 tetrahedra and M/TO_8 distorted square antiprisms [3,7]. Along *a* and *b* directions it is built of parallel chains of alternate, edge-sharing M/TO_8 and XO_4 polyhedra, of only one type in each row, and in the *c* direction M/TO_8 polyhedra from two different consecutive chains are linked through a common face, forming $(M/T)_2O_{12}$ dimeric units. For laser applications it is essential that further (inhomogeneous) spectral broadening can be expected for the $I\bar{4}$ structure due to the random distribution of Yb/Gd/La and Li/Na cations over two nonequivalent (2*b* and 2*d*) sites with specific occupancy factors [3,8] while for the $I4_1/a$ space group this distribution is over a single site (4*b*) with an occupancy factor of 0.5.

3. Spectroscopy of Yb^{3+} ions in $MT(XO_4)_2$ single crystals

Since ytterbium lasers operate as a quasi 3-level system it is important to know the splitting of the ground $^2F_{7/2}$ manifold. Energy level schemes for the four hosts NaGdW, NaLaW, NaLaMo and LiGdMo were derived from unpolarized and polarized (π, $E\|c$ and σ, $E\perp c$) absorption and emission measurements in the 5–300 K temperature range (Table 1).

The crystal field splitting is rather similar for the four hosts and for the ground multiplet it is only 10–20% smaller than in the monoclinic $KY(WO_4)_2$ and $KGd(WO_4)_2$ [2]. The inhomogeneous contribution to the linewidth broadening in disordered hosts can be most easily seen for the zero-phonon (0) $^2F_{7/2} \leftrightarrow (0')\ ^2F_{5/2}$ transition at low (5 K) temperature. While the FWHM of this line is 3.5 cm^{-1} for typical ordered monoclinic double tungstate hosts like $KGd(WO_4)_2$ which possess a unique site for Yb^{3+}, it amounts, e.g., to ≈11 cm^{-1} for Yb:NaLaMo, ≈13 cm^{-1} for Yb:NaGdW and ≈14 cm^{-1} for Yb:LiGdMo. Table 2 shows the maximum room temperature absorption cross sections and the fluorescence lifetimes.

In general, the peak absorption is higher for the π-polarization. While this normally results also in higher emission cross sections at the same wavelength it does not necessarily mean that the gain cross section (the difference of the emission and absorption cross sections multiplied by the corresponding populations) is higher at longer wavelengths where laser operation should be expected because of the role of the residual absorption. The lifetimes in Table 2

Table 1
Excited energy levels of the lower ($^2F_{7/2}$) and upper ($^2F_{5/2}$) Yb^{3+} multiplets measured in cm^{-1} from the ground state (0) $^2F_{7/2}$

Host\level	(1) $^2F_{7/2}$	(2) $^2F_{7/2}$	(3) $^2F_{7/2}$	(0′) $^2F_{5/2}$	(1′) $^2F_{5/2}$	(2′) $^2F_{5/2}$
NaGdW	218	383	500	10276	10410	10658
NaLaW	177	328	462	10271	10356	10645
NaLaMo	175	353	498	10256	10351	10638
LiGdMo	216	376	480	10263	10380	10647

Table 2
Absorption peak (zero-phonon transition), the corresponding cross-sections for the two polarizations (π and σ) and fluorescence lifetime τ in the studied disordered Yb-hosts

Yb-host	λ_{max} [nm]	$\sigma_{\pi,max}$ [10^{-20} cm^2]	$\sigma_{\sigma,max}$ [10^{-20} cm^2]	τ [μs]
NaGdW	974	1.51	1.21	320
NaLaW	976	1.60	1.15	220
NaLaMo	977	2.5	1.5	280
LiGdMo	975	1.64	1.17	250

are comparable or even larger than in the monoclinic double tungstates.

4. Laser experiments

All laser experiments described in this section were performed with uncoated samples whose axis location permitted to study both π- and σ-polarization (either exactly or very close to the appropriate orientation). Four different pump sources were used: a broadly tunable cw Ti:sapphire laser (960–1025 nm, linewidth < 1 nm, max 3 W), a polarized tapered diode laser with simple shaping optics (975–982 nm, linewidth = 1 nm, max 2 W, $M^2 < 3$ for the slow axis emission) and unpolarized 8 W (974–980 nm, multipeak bandwidth ≈8 nm, 116 μm fiber core diameter, NA = 0.2) and 50 W (980 nm, linewidth: 4 nm, 200 μm fiber core diameter, NA = 0.22) fiber-coupled diode laser modules. The samples were mounted on copper holders and only in the last case water cooling was applied to maintain the room temperature.

The three-mirror astigmatically compensated laser cavity (Fig. 1(a)) with Brewster angle geometry was used for pumping with the Ti:sapphire or the tapered diode laser. It consisted of an end mirror M_1 with radius of curvature RC = −5 cm, a folding mirror M_2 with RC = −10 cm,

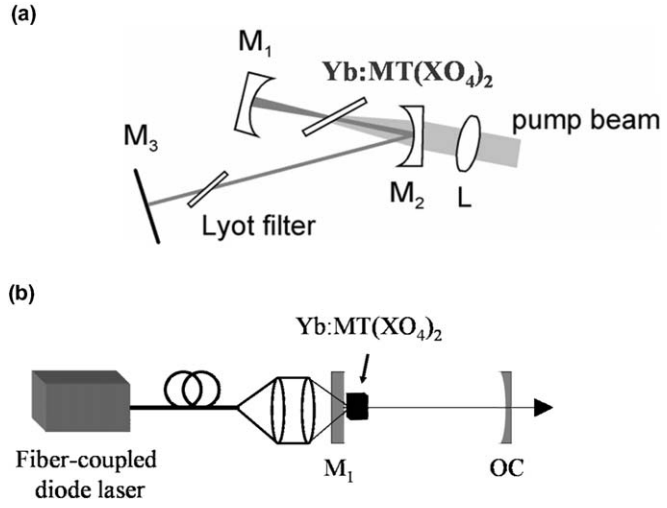

Fig. 1. Schematics of the laser setup: (a) three-mirror cavity for pumping with the Ti:sapphire or the tapered diode laser; (b) plane-concave cavity for pumping with the fiber-coupled diode modules.

through which the pump beam was focused by a f = 6.28 cm lens L, and a plane output coupler (M_3) of transmission T_{OC}. The total cavity length was about 70 cm. The pump beam focal spot had a Gaussian waist of about 22 μm in the case of Ti:sapphire laser pumping which resulted in general in stronger bleaching of the absorption.

In order to obtain higher output powers the hemispherical cavity shown in Fig. 1(b) was used with the fiber coupled diode modules. M_1 was a plane high reflector for the laser wavelength (1020–1200 nm) on a 3-mm-thick quartz substrate which was highly transmitting near 980 nm and the concave output coupler (OC) had RC = −5 cm. The sample was placed as close as possible (≈0.2 mm) to M_1. The unpolarized pump beam was focused to a spot size of ≈40 μm (Gaussian waist) by a f = 6.2 mm microoptics in the case of the high brightness and to about 100 μm using 1:1 imaging optics in the case of the 50 W fiber coupled diode module.

Table 3 summarizes the results obtained for the π-polarization. Fig. 2 gives a comparison of the output power for Ti:sapphire laser pumping with the linear fits for calculation of the slope efficiency η. This graph reflects the situation at present and the results achieved with the different hosts depend strongly on the crystal quality which was best for LiGdMo. It is obvious that the lowest threshold corresponds to the lowest doping level. The results obtained for the σ-polarization were slightly lower in terms of output power but the efficiencies with respect to the absorbed power were almost the same. Also the generation wavelength (λ_L) was slightly different for the two polarizations which means that the gain maximum occurs at a different wavelength. For both polarizations λ_L decreased with increasing T_{OC}. Thus it can be expected that for practical applications also the σ-polarization may be preferable. This is related to the opto-mechanical properties and the heat flow which is expected to be more homogeneous for active elements cut along the symmetry axis.

Fig. 3(a) shows the results obtained in the same cavity configuration with the same Yb:LiGdMo sample pumped by the tapered diode laser. The absorption bleaching was rather low in this case. The results can be directly compared with Fig. 2 and obviously the lower quality of the pump beam profile results in lower efficiencies and output powers, and the threshold is increased.

The output powers could be scaled by pumping with the high brightness 8 W fiber coupled diode laser module in the cavity shown in Fig. 1(b) and up to 900 mW could be achieved with Yb:NaLaMo at 1035 nm (Fig. 3(b)). Also in this case the bleaching of the absorption was rather low. The results depended on the crystalline quality (better for Yb:NaLaMo than for Yb:NaLaW), the parallelism of the samples, and the absorption. The absorption could be estimated only under nonlasing conditions because of the strong pump divergence behind the sample. It was about 40% in Yb:NaLaMo and 35% in Yb:NaLaW at an incident power of 3.5 W but decreased by roughly 8% in both cases for the maximum pump levels in Fig. 3(b) due to

Table 3
Yb-laser parameters (π-polarization) achieved with polarized Ti:sapphire and unpolarized fiber-coupled diode pump lasers

Host	Ti:sapphire laser pumping				Diode laser pumping		
	NaGdW	NaLaW	NaLaMo	LiGdMo	NaLaW	NaLaMo	LiGdMo[a]
λ_P [nm]	973.6	976.6	976.7	975	≈976	≈976	980
T_{OC} [%]	10.0	1.1	1.1	10.0	1.0	1.0	5
P_{max} [mW]	336	205	400	473	330	900	660
λ_L [nm]	1026.8	1034	1039.5	1025.7	1031	1035	1027
$\Delta\lambda$ [nm]	33	40	48	23			

λ_P: Pump wavelength, T_{OC} and λ_L for maximum output power P_{max}, $\Delta\lambda$: full tunability range with Lyot filter.
[a] Crystal with active cooling.

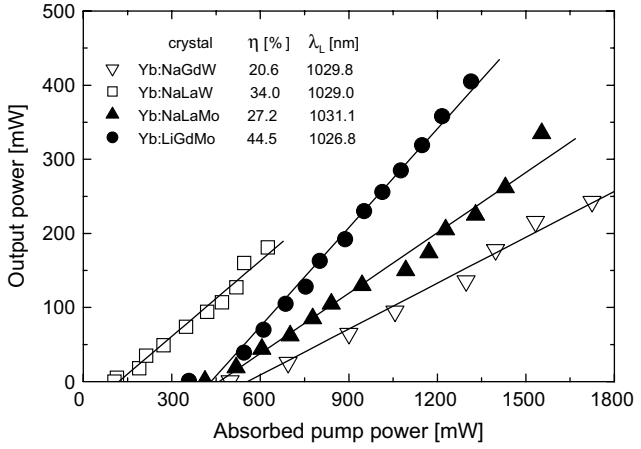

Fig. 2. Laser performance of Yb-doped NaGdW (3.3 mm thick), NaLaW (3.4 mm thick), NaLaMo (2.6 mm thick), and LiGdMo (2.6 mm thick) crystals under Ti:sapphire laser pumping using the cavity from Fig. 1(a) with $T_{OC} \approx 3\%$ (π-polarized pump and laser).

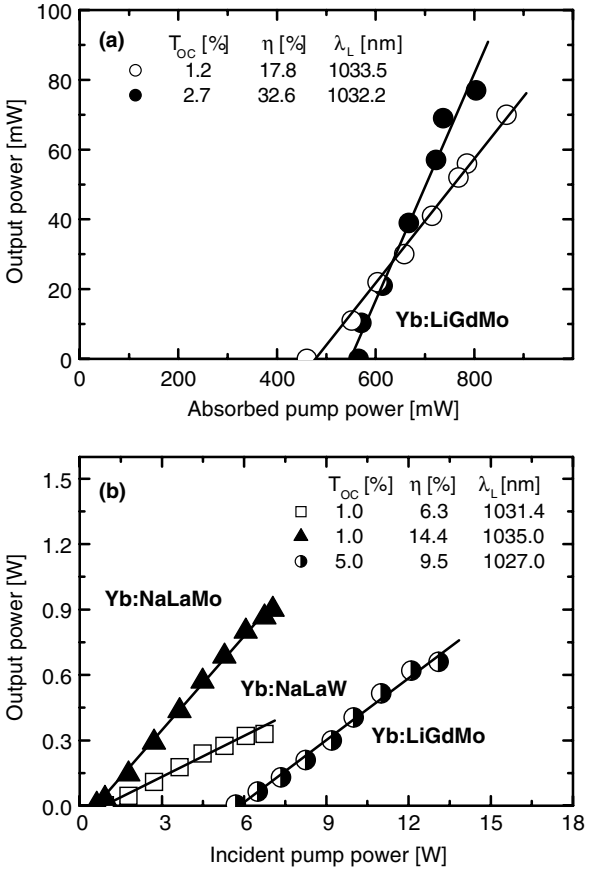

Fig. 3. Diode pumped laser performance of Yb-doped disordered crystals: (a) Yb:LiGdMo (2.6 mm thick) pumped at 975 nm with the tapered diode laser in the cavity from Fig. 1(a) (π-polarized pump and laser); (b) Yb:NaLaW (3.4 mm thick) and Yb:NaLaMo (2.6 mm thick) crystals pumped at 976–977 nm by the high-brightness 8 W fiber coupled diode module and Yb:LiGdMo (1.9 mm) crystal pumped at 980 nm by the 50 W fiber coupled diode module. The Yb-laser is π-polarized in all cases.

the changing pump spectrum. Since the absorbed power could not be precisely estimated, the slopes in Fig. 3(b) were calculated with respect to the incident pump power and are correspondingly lower. The situation was similar for the pumping of the Yb:LiGdMo sample (cut from the same boule) in Fig. 3(b) with the 50 W fiber coupled diode module. Although the spectral linewidth and shape were much better for this pump source, the deviation of its fixed wavelength from the absorption maximum (the absorption was only about 37%, compare Tables 2 and 3) and the larger pump spot size resulted in increased thresholds and lower slope efficiencies with respect to the incident pump power.

The laser tunability was studied only by Ti:sapphire laser pumping inserting a two-plate Lyot in the cavity arm containing the output coupler (Fig. 1(a)). Fig. 4 summarizes the results obtained for the π-polarization. In all cases the tunability was limited on the short-wavelength side by the transmission characteristics of the output couplers. The largest tunability (48 nm) was obtained with Yb:NaLaMo (Fig. 4(a), Table 3). The FWHM in this case corresponds to 9.1×10^{12} Hz which means that potentially sub-50 fs can be supported in a mode-locked laser. The other hosts are compared in Fig. 4(b) and Table 3. Smaller output coupling extended the tunability in Yb:NaGdW but the results for the two polarizations were quite similar. For Yb:LiGdMo the σ-polarization has an extended tuning range further to longer wavelengths.

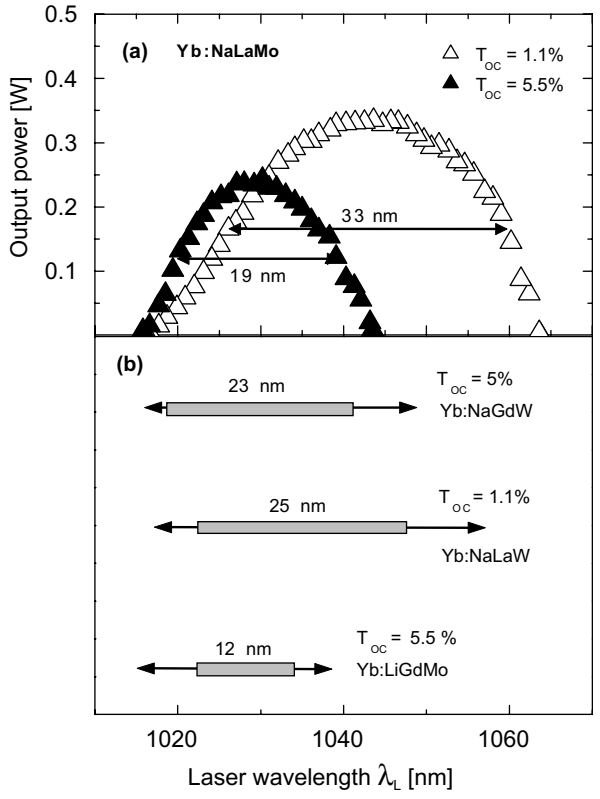

Fig. 4. Wavelength tunability under Ti:sapphire laser pumping in π-polarization. (a) Yb:NaLaMo (2.6 mm thick) output power with two different output couplers for an absorbed power of 1.4 W, and (b) full tuning ranges (arrows) and FWHM of the tuning curves (boxes and numbers) achieved with Yb:NaGdW (3.3 mm thick, absorbed power: 1.7 W), Yb:NaLaW (3.4 mm thick, absorbed power: 0.75 W) and Yb:LiGdMo (2.6 mm thick, absorbed power: 1.5 W).

5. Conclusion

In conclusion, disordered uniaxial crystals of NaGdW, NaLaW, NaLaMo and LiGdMo with tetragonal structure, were successfully grown with sufficient Yb-doping and optical quality. The crystal field splitting of the Yb^{3+} multiplets and the lifetimes are similar to the biaxial monoclinic double tungstates but the peak absorption cross sections are roughly one order of magnitude lower. Room temperature and tunable cw laser operation was obtained under Ti:sapphire laser pumping and power scaling was achieved by pumping with different laser diodes. The slope efficiency with the best quality sample (Yb:LiGdMo) reached 64.5% (for $T_{OC} = 10\%$) and the maximum output power obtained with Yb:NaLaMo was 900 mW. The observed tunability (e.g., FWHM = 33 nm) is promising for mode-locked femtosecond operation.

Acknowledgements

This work was supported by the European Commission under Project DT-CRYS (STRP-505580-1). We acknowledge also financial support through Projects MAT 2002-4605-C05-05, CAM-MAT-434-2004 (Spain), and the Education and Science Ministry of Spain (M. Rico: EX2003-0784, X. Han: SB2003-0232).

References

[1] V.K. Trunov, V.A. Efremov, J.A. Velikodnyj, Kristallochimija i svojstva dvojnych molibdatov i vol'framatov, Nauka, Leningrad, 1986 (in Russian).
[2] N.V. Kuleshov, A.A. Lagatsky, A.V. Podlipensky, V.P. Mikhailov, G. Huber, Opt. Lett. 22 (1997) 1317.
[3] C. Cascales, A. Méndez Blas, M. Rico, V. Volkov, C. Zaldo, Opt. Mater. 27 (2005) 1672.
[4] M. Rico, J. Liu, U. Griebner, V. Petrov, M.D. Serrano, F. Esteban-Betegón, C. Cascales, C. Zaldo, Opt. Exp. 12 (2004) 5362.
[5] M. Rico, J. Liu, J.M. Cano-Torres, A. García-Cortés, C. Cascales, C. Zaldo, U. Griebner, V. Petrov, Appl. Phys. B 81 (2005) 621.
[6] M.D. Serrano, F. Esteban-Betegón, C. Zaldo, J. Cryst. Growth 275 (2005) e819.
[7] M. Rico, U. Griebner, V. Petrov, P. Ortega, X. Han, C. Cascales, C. Zaldo, J. Opt. Soc. Am. B, in press.
[8] V. Volkov, C. Cascales, A. Kling, C. Zaldo, Chem. Mater. 17 (2005) 291.
[9] J. Liu, J.M. Cano-Torres, F. Esteban-Betegón, M.D. Serrano, C. Cascales, C. Zaldo, M. Rico, U. Griebner, V. Petrov, Opt. Laser Technol., in press.
[10] A.S. Yasukevich, A.V. Mandrik, V.E. Kisel, V.G. Shcherbitsky, G.N. Klavsut, N.V. Kuleshov, A.A. Pavlyuk, OSA trends in optics and photonics (TOPS), Advanced Solid-State Photonics, vol. 98, Optical Society of America, Washington, DC, 2005, p. 167.
[11] J. Johannsen, M. Mond, K. Petermann, G. Huber, L. Ackermann, D. Rytz, C. Dupre, Advanced solid-state photonics, Vienna, Austria, February 6–9, 2005, Tech. Dig. (CD ROM), Paper MB44.